2014 IEEE/RSJ International Conference on
Intelligent Robots and Systems (IROS 2014)
September 14-18, 2014, Chicago, IL, USA

A Sequence of Micro-assembly for Irregular Objects Based on a Multiple Manipulator Platform

Dengpeng Xing, De Xu, and Haipeng Li

Abstract— **Difficulties arise in the micro-assembly of many irregular objects and in the insertion with contact between components of soft materials. To handle these problems, we design a micro-operational platform with multiple manipulators to facilitate a sequence of assembly. Six robot arms and three microscopes are incorporated, together with macro and micro motion systems. We also propose a hybrid control strategy to achieve high precision and protect objects. This hybrid scheme includes vision based positioning controllers for alignment, which employ incremental PI controllers and image Jacobian matrix, force based controllers for insertion, and a decision mechanism determining the assembly state. Experiments demonstrate the effectiveness of the proposed platform and control methods.**

I. INTRODUCTION

Micro-assembly draws much attention in the field of robotics since it can provide high precision and operate on small objects [1], [2].

New types of platforms were recently presented to fulfill different kinds of tasks. Khalil [3] used a cluster of paramagnetic microparticles to carry out a wireless two-dimensional microassembly operation. A magnetic-based manipulation system was used to control the motion of the cluster under the influence of the applied magnetic fields. Bolopion [4] presented teleoperated 3-D microassembly of spherical objects with haptic feedback. He used a dual-tip gripper to pick-and-place microspheres whose diameter is approximately $4 \sim 6\mu m$. In Ref. [5], the new development of a 6 degree of freedom robotic manipulator was used in the assembly of three-dimensional MEMS microstructures. A flexible, multi-scale test-bed was developed [6] for use in conjunction with caging micro-manipulation motion primitives for 2D and 3D autonomous micro-assembly tasks.

In micro-assembly, vision-based control methods are commonly used, which can be categorized into three types: position-based, image-based, and hybrid scheme. Wason [7] used multiple coordinated probes for micro assembly with automated vision-guided. He developed the capabilities required for construction of 3D structure using only planar micro fabricated parts. Tamadazte [8] investigated sequential robotic micromanipulation and microassembly using a monoview and multiple scale 2-D visual control scheme. The imaging system was a photon video microscope endowed with an active zoom enabling to work at multiple scales. In Ref. [9], a visual-servo-control approach was used to automatically perform micro-grasping and micro-joining in sequence.

Calibration is needed for the microscopic system in order to accurately control the manipulators. A class of miniature vision sensors was proposed and analyzed that enabled a wide field-of-view within a small form through a refractive optical design [10]. To calibrate stereo microscope, Wang [11] estimated the main parameters and rectification parameters of an imaging model using the symmetry and the differences between the two optical paths of stereo microscopic vision system. Cheah [12] presented a simple vision based setpoint controller with adaptation to uncertainty in depth information. Our previous work presented an active calibration method for platforms with multiple manipulators [13].

In contact assembly, force-based control strategies are also employed. Two approaches were described [14] for precision position and force control to grip micro objects. One is a position-based sliding mode impedance control method and the other is based on a proportional-integral type of sliding function of the impedance measure error. Rabenorosoa [15] used a two-sensing-fingers gripper to grasp planar microparts and analyzed the lateral contact force which was estimated less than 3mN. In Ref. [16], a hybrid micro assembly technique was reported to combine a robotic micromanipulator and a water droplet self-alignment.

Most research focuses on micro-operation of one manipulator (such as grippers, pick-and-place tasks) or micro-assembly of two objects (commonly peg-in-hole), whereas micro-assembly of many components remains open. This paper investigates this sequence of micro-assembly of multiple irregular objects. We design a micro-operational platform equipped with multiple manipulators to accomplish this task and develop a hybrid control strategy to achieve the required precision and protect thin objects. The hybrid scheme includes vision based controllers for alignment, force controllers for insertion, and a decision mechanism to determine the assembly state. We accomplish micro-assembly of four components in experiments, which verifies the effectiveness of the proposed platform and control methods.

The rest of the paper is organized as follows. Section II describes the components to be assembled and the assembly process. In Section III, a platform is designed to complete this assembly task meeting the requirements and solving the difficulties. Section IV addresses the control strategy, and experiments are carried out on the platform in the next section. The paper is concluded in Section VI.

Dengpeng Xing, De Xu, and Haipeng Li are with Institute of Automation, Chinese Academy of Sciences, Beijing, China. (e-mail: dengpeng.xing@ia.ac.cn)

978-1-4799-6934-0/14/$31.00 ©2014 IEEE

II. THE ASSEMBLY TASK

A. The components

The four components to be assembled and their assembly relationships are shown in Fig. 1, and Tab. I displays the details of each component. The distinctions of these assemblies are discussed as following: 1) The objects are irregular shaped and all thin: A, B, and C are approximately 0.5-1 mm thickness and the diameter of D is about 0.1mm. Specific end-effectors are then needed to hold them. 2) The components A, B, and C are made of soft materials, therefore this task includes soft assembly and too large force leads to deformation. 3) From Tab. I, it is also known that three assemblies consist of three different fit types, wherein interference fit inevitably generates forces between objects. 4) High precision requirements, $5\mu m$ in positioning and 0.1° in posture. 5) A long distance insertion lies in the assembly of A and B, which may cause deviations in positioning and posture. 6) To automatically accomplish these four objects assembly on one platform, appropriate placement of each manipulator and coordinated control are needed in order to share the small micro-operation space.

Especially these difficulties all lie in the assembly of components A and B, which becomes the main focus of this paper. Since the objects A and D are loose (clearance fit) after assembly, we need a needle containing glue to dispense between objects A and D. This dispensing needle is labeled as component E in this paper.

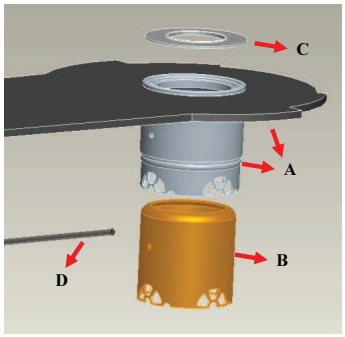

Fig. 1. The components and their assembly relationships.

TABLE I
THE DETAILS OF THE COMPONENTS.

	object A	object B	object C	object D
shapes	cylindrical hollow	cylindrical hollow	insert	long thin needle
assembly relationships	B, C, D	A	A	A & B
fit types		interference fit	transition fit	clearance fit

B. The assembly process

The assembly target is to put the component B into A with holes on them being aligned, to insert object D into the small hole of the assembly of A and B, and to place the object C into the upper hole of A. Considering the characteristics of these objects, we arrange an assembly sequence to complete this target as described in Fig. 2. Each sub-assembly needs to move objects into the micro-operation space, to extract features and determine the state of the components, to align their postures and positions, and then to start the insertion. Since the black part of the component A is larger than its own cylindrical structure, the assembly of A and B is inverted so as to facilitate the upper camera to observe insertion of the object D.

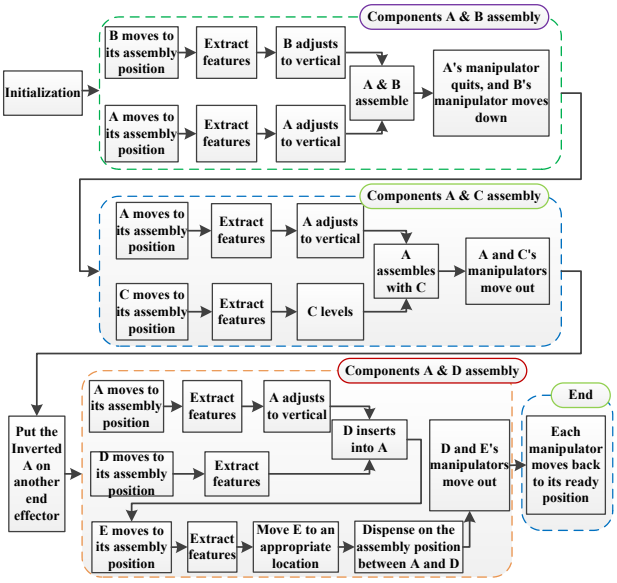

Fig. 2. The assembly process.

III. THE PLATFORM SYSTEM DESIGN

To complete the assembly of the above components, considering the mentioned difficulties, we need a micro-operation platform with multiple manipulators. Six robot arms are required to hold the objects A∼E and an inverted A, and specific clampers are demanded to hold the irregular and thin components.

This is an obvious three dimensional assembly, therefore at least three microscopes are used for vision feedback. Since the micro camera has the characteristics of small view depth and small view field, this mechanism also needs macro actuators in order to share the micro operational space among the multiple robot arms without interference, and micro motion systems to adjust their movements in the view of microscopes. In addition, micro movable vision systems are required to actively adjust the interested view plane and to increase the clear view area of the vision system.

Fig. 3 shows the platform model, which has 40 DoFs totally. Each robot arm is provided with a translational rail to fulfill macro movement. The arm 6 has a vertical translational DoF and three rotational DoFs, while the others all have three micro translational DoFs. The arms 4, 5, and 8 are equipped with roll & pitch rotational mechanisms to manually adjust

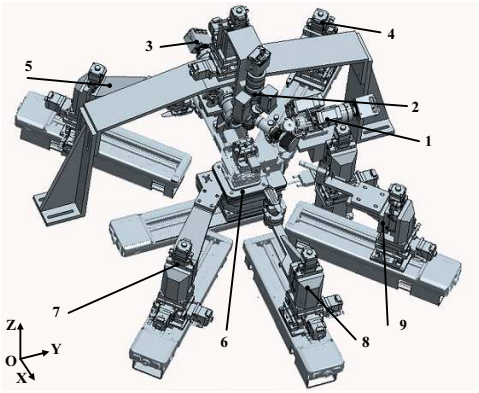

Fig. 3. The platform model for complex components assembly. Subsystems 1∼3 are the microscopes and 4∼9 are the robot arms.

the end effector's posture, and the arms 4 and 8 have micro-force sensors in order to handle soft assembly and protect thin objects. Two cameras are placed in horizontal plane and one is located on the top, and each microscope has a micro movement unit with three dimensional DoFs.

The component A and its inverted are held by the manipulators 5 and 8, individually; the object C is clamped by the robot arm 4; and part D is fixed on the the end-effector of the arm 7. Vacuum absorptive mechanisms are designed to hold these irregular and thin objects. The component B is put on the manipulator 6 and the dispensing needle E is on the robot arm 9. The dispensing power is also supplied by a vacuum mechanism.

The world coordination is also established: the y-axis is defined as the arm 6 moving to the micro-operational space along its rail; the x-axis is orthogonal to y-axis in the horizontal plane with the positive direction defined as actuating the arm 8 outside; and the z-axis is determined by the right-hand rule. The operational coordination is fixed on each robot arm with y-axis along with the rail direction and z-axis being the vertical to facilitate the assembly.

In Fig. 3, we put the camera 1 to be parallel with the y-axis, the camera 2 with the z-axis, and the camera 3 with the x-axis. But the cameras are not strictly orthogonal; they can also be placed at certain positions or postures so that interested features are in their clear view. Each robot arm is just located in order to facilitate assembly in the micro space, according to the irregular objects they grip.

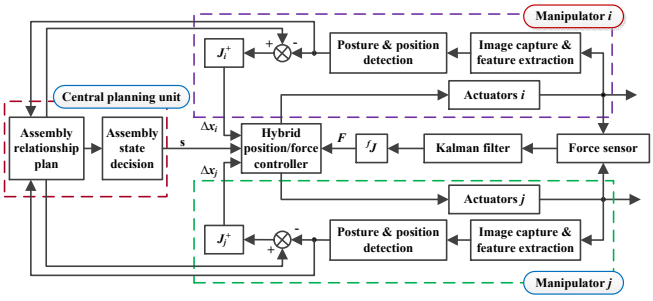

Fig. 4. The control strategy of micro-assembly between two components.

TABLE II

THE NOTATIONS USED IN THIS PAPER.

The label	The meaning
$\boldsymbol{s}$	Assembly state matrix
${}^{f}\boldsymbol{J}$	Force Jacobian matrix
${}^{i}\boldsymbol{J}_{j}$	Image Jacobian matrix of the j^{th} manipulator in the i^{th} microscope view
$[\Delta u_i, \Delta v_i]^{\mathrm{T}}$	Image Jacobian matrix in the i^{th} microscope
$[\Delta x_j, \Delta y_j, \Delta z_j]^{\mathrm{T}}$	Relative movement of the j^{th} manipulator
$\boldsymbol{g}_{ki}$, $\boldsymbol{g}_{kj}$	Switch functions for alignment in k^{th} subassembly
$\boldsymbol{g}_{kf}$	Switch functions for insertion in k^{th} subassembly
K_{pi}, K_{ii}	Proportional and integral factors of i controller
λ_{a}	One step length of adjusting
λ_{bz}	Step length of the insertion
f_{T}	Force threshold
$[\Delta \mathrm{x_a}, \Delta \mathrm{y_a}]^{\mathrm{T}}$	Horizontal change of component A
$\Delta \mathrm{z_b}$	Insertion movement of object B

IV. CONTROL STRATEGY

A. The control mechanism

The assembly with contact between components needs a hybrid controller including vision based alignment and force based insertion, the control strategy of which is shown in Fig. 4, while the others only needs visual positioning and alignment. The notations used in this section is displayed in Tab. II.

During the assembly, in Fig. 4, the vision unit extracts features from the image captured by the microscopic system and separates components. After acquiring the position and posture of each object in the view of the corresponding cameras, they are fed into the assembly relationship plan, where the desired state of each manipulator is determined according the assembly planning. The image state errors multiplying image Jacobian matrix lead to the desired relative movements of the corresponding manipulators. These motor commands are sent into the controller. At the same time, the force sensor detects the forces between the components, which are filtered by Kalman filter. After multiplying the force Jacobian matrix, force information is also fed into the controller. Another input of the hybrid controller comes from the assembly state decision, which decides the state of the assembly (alignment or insertion, and in which assembly) according to the assembly relationship. The controller output drives the corresponding actuators.

According to the assembly relationship plan and the current state, the decision mechanism determines the assembly state. If the posture and position errors between components reach the alignment precision requirement, the alignment is then accomplished and the the assembly state changes from "alignment" to "insertion". If the previous "insertion" satisfies the desired criterion, the assembly state switches to the next assembly. The assembly state matrix is expressed as $\boldsymbol{s} = [\boldsymbol{s}_1^{\mathrm{T}}, \boldsymbol{s}_2^{\mathrm{T}}, \boldsymbol{s}_3^{\mathrm{T}}]^{\mathrm{T}}$, where $\boldsymbol{s}_{\mathrm{k}} = [\mathrm{s_{ka}}, \mathrm{s_{ki}}]$ indicates the state of k's sub-assembly, $k = 1$ means the state of assembly of A and B, $k = 2$ indicates the state of A and C assembly, and $k = 3$ shows the state of assembly of A and D, $\mathrm{s_{ka}}$ and $\mathrm{s_{ki}}$ are the state indications of "alignment" and "insertion". Only an

element of this matrix $\boldsymbol{s}$ is one during the assembly, and the others are all zero.

Two Jacobian matrices are employed in the control strategy. One is force Jacobian matrix ${}^{f}\boldsymbol{J}$, which is to map from the coordination of force sensor to the coordination of manipulator. The other is image Jacobian matrix.

B. Image Jacobian matrix

Positioning based on visual feedback is used for alignment. For visual servo, we employ Hough transformation to extract features, and image Jacobian matrix to transform from the image changes to the motor movements in the Cartesian space.

For any point in the end-effector of any manipulator, the relative movements in Cartesian space have only a scale to their position changes in the eye of the microscope. Without considering rotational DoFs, the relation can be written as

$$\begin{bmatrix} \Delta u_i \\ \Delta v_i \end{bmatrix} = {}^{i}\boldsymbol{J}_j \begin{bmatrix} \Delta x_j \\ \Delta y_j \\ \Delta z_j \end{bmatrix}, \tag{1}$$

where ${}^{i}\boldsymbol{J}_j \in \mathbb{R}^{2\times 3}$.

To solve the above equation, we use the least square method,

$${}^{i}\boldsymbol{J}_j = \boldsymbol{A}_i \boldsymbol{B}_j^{\mathrm{T}} (\boldsymbol{B}_j \boldsymbol{B}_j^{\mathrm{T}})^{-1}, \tag{2}$$

where

$$\boldsymbol{A}_i = \begin{bmatrix} \Delta u_{i1} & \Delta u_{i2} & \cdots & \Delta u_{in} \\ \Delta v_{i1} & \Delta v_{i2} & \cdots & \Delta v_{in} \end{bmatrix},$$

$$\boldsymbol{B}_j = \begin{bmatrix} \Delta x_{j1} & \Delta x_{j2} & \cdots & \Delta x_{jn} \\ \Delta y_{j1} & \Delta y_{j2} & \cdots & \Delta y_{jn} \\ \Delta z_{j1} & \Delta z_{j2} & \cdots & \Delta z_{jn} \end{bmatrix},$$

and n is the total trials. Equation (2) has solution if and only if matrix $\boldsymbol{B}$ is full rank; and since the matrix $\boldsymbol{B}$ is a $3 \times n$ matrix, the sufficient and necessary condition to compute the Jacobian is $n \geq 3$, i.e., the active motions include at least three steps. More recorded motions can improve the calibration accuracy.

A microscope is only sensitive to two translational DoFs, therefore two cameras are at least required to determine the exact motion without multiple solutions. Using the Jacobian matrix, we can compute the corresponding manipulator motion given the required tasks in each individual camera. For the j^{th} arm, the expected manipulator movement is

$$\begin{bmatrix} \Delta x_j \\ \Delta y_j \\ \Delta z_j \end{bmatrix} = \begin{bmatrix} {}^{1}\boldsymbol{J}_j \\ \vdots \\ {}^{m}\boldsymbol{J}_j \end{bmatrix}^{\dagger} \begin{bmatrix} \Delta u_1 \\ \Delta v_1 \\ \vdots \\ \Delta u_m \\ \Delta v_m \end{bmatrix}, \tag{3}$$

where $\boldsymbol{J}_j = [{}^{1}\boldsymbol{J}_j^{\mathrm{T}}, \cdots, {}^{m}\boldsymbol{J}_j^{\mathrm{T}}]^{\dagger}$ is the Jacobian matrix mapping the j^{th} robot arm motion to the image coordination changes in the microscopic vision system, † means the pseudo-inverse, and m is the number of microscopes.

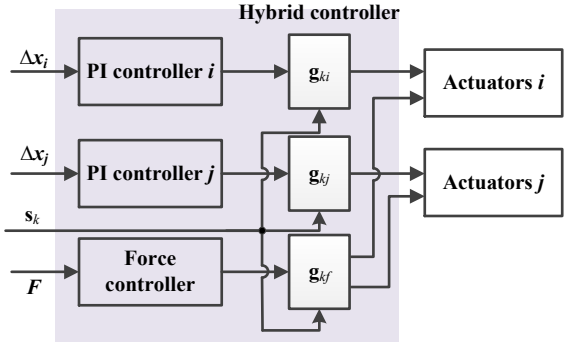

Fig. 5. The hybrid vision/force controller.

C. Hybrid controller

The hybrid controller generates motor commands according to its inputs, i.e., the image state errors, the force between components, and the assembly state matrix. This hybrid structure has two types of controllers, which are used for vision based positioning and force based insertion, respectively, as shown in Fig. 5. The decision system picks a controller according to the current assembly state. The switch mechanism is written as

$$\begin{aligned} \boldsymbol{g}_{ki} = \boldsymbol{g}_{kj} &= \begin{cases} 1, & \mathrm{s_{ka}} = 1 \\ 0, & \mathrm{s_{ka}} = 0 \end{cases}, \\ \boldsymbol{g}_{kf} &= \begin{cases} 1, & \mathrm{s_{ki}} = 1 \\ 0, & \mathrm{s_{ki}} = 0 \end{cases}. \end{aligned} \tag{4}$$

The decision mechanism only activates one controller for use at a time. Fusion control is not applied since vision based positioning is not available due to the cover between objects and deformation, and force controller can supply high precision of insertion.

If the assembly is in the state of alignment, visual servo is activated and incremental proportional-integral (PI) controllers are used to drive motors according to the visual state errors. The control law from visual states to motor motion is written as

$$\begin{aligned} \begin{bmatrix} \Delta x_{ik} \\ \Delta y_{ik} \\ \Delta z_{ik} \end{bmatrix} &= \mathrm{K_{pi}} \boldsymbol{J}_i^{\dagger} \left(\begin{bmatrix} \Delta u_{1k} \\ \Delta v_{1k} \\ \cdots \\ \Delta u_{mk} \\ \Delta v_{mk} \end{bmatrix} - \begin{bmatrix} \Delta u_{1(k-1)} \\ \Delta v_{1(k-1)} \\ \cdots \\ \Delta u_{m(k-1)} \\ \Delta v_{m(k-1)} \end{bmatrix} \right) \\ &\quad + \mathrm{K_{ii}} \boldsymbol{J}_i^{\dagger} \begin{bmatrix} \Delta u_{1k} \\ \Delta v_{1k} \\ \cdots \\ \Delta u_{mk} \\ \Delta v_{mk} \end{bmatrix}, \end{aligned} \tag{5}$$

where k is sampling time.

If the insertion is started, the hybrid system is then changed to a force based controller, which adjusts the component's positions according to the force detected by the sensors, in order to reduce the forces and protect the objects. The controller stops insertion and adjusts one object's position if the horizontal force detected is too large. The

insertion continues after the force is less than the threshold. This insertion controller can be expressed as a combination of an adjusting controller, an insertion controller, and a stop controller.

$$\begin{bmatrix} \Delta x_a \\ \Delta y_a \\ \Delta z_b \end{bmatrix} = \begin{cases} \begin{bmatrix} \lambda_{ax}\mathrm{sig}(f_x) \\ \lambda_{ay}\mathrm{sig}(f_y) \\ 0 \end{bmatrix}, & [(|f_y| > |f_{Ty}|)||(|f_y| > |f_{Ty}|)] \\ & \&(|f_z| \le |f_{Tz}|) \\ \begin{bmatrix} 0 \\ 0 \\ \lambda_{bz} \end{bmatrix}, & (|f_x| \le |f_{Tx}|)\&(|f_y| \le |f_{Ty}|) \\ & \&(|f_z| \le |f_{Tz}|) \\ \begin{bmatrix} 0 \\ 0 \\ 0 \end{bmatrix}, & |f_z| > |f_{Tz}| \end{cases} \tag{6}$$

where λ_{ax} and λ_{ay} are the adjusting magnitudes in horizon plane, the values of which are determined by

$$\begin{cases} \sqrt{\lambda_{ax}^2 + \lambda_{ay}^2} = \lambda_a, \\ \frac{\lambda_{ax}}{\lambda_{ay}} = \frac{|f_x|}{|f_y|}, \end{cases}$$

f is the force after multiplying the force Jacobian matrix, and

$$\mathrm{sig(x)} = \begin{cases} 1, & x > 0 \\ 0, & x = 0 \\ -1. & x < 0 \end{cases}$$

V. EXPERIMENTS

A. Experiment system

We have established a platform according to the scheme given in Section III, as shown in Fig. 6. Two GC2450 cameras and one PointGrey camera constituted the microscopic system, and each camera was equipped with Navitar lens. The macro rails were Sigma SGSP26-200, with repeatability resolution as $\pm 3\mu$m. All three dimensional DoFs sub-platforms were Suguar KWG06030-G, the translational resolution of which was $\pm 0.5\mu$m. In robot arm 6, the vertical elevation stage was Micos ES-100 with movement errors within 0.1μm, and the three rotational motors were KGW06050-L around its x-axis and y-axis, and SGSP-40yaw around z-axis. On the end-effectors of arms 4, 5, and 8, tilt stages Sigma KKD-25C were placed to manually adjust the component's postures. The force sensors were Nano-43, with measurement ranging between $\pm$18N and resolution as 1/128N.

B. The image Jacobian results

We picked the robot arm 4 as an example in this calibration process. This manipulator had three micro translational DoFs and horizontal cameras were used to form the microscopic vision system. The equation (2) had solution if and only if $\mathrm{R}(\mathbf{B}) = 3$, i.e, at least three steps of active motions were required. This manipulator was then actuated for 6 steps and the image coordination change of an interested feature were recorded in each camera. Moving in the view area of the camera 3, we had

$$\mathbf{B}_4 = \begin{bmatrix} 500 & 0 & 0 & -500 & 0 & 0 \\ 0 & 500 & 0 & 0 & -500 & 0 \\ 0 & 0 & 500 & 0 & 0 & -500 \end{bmatrix} \mu m,$$

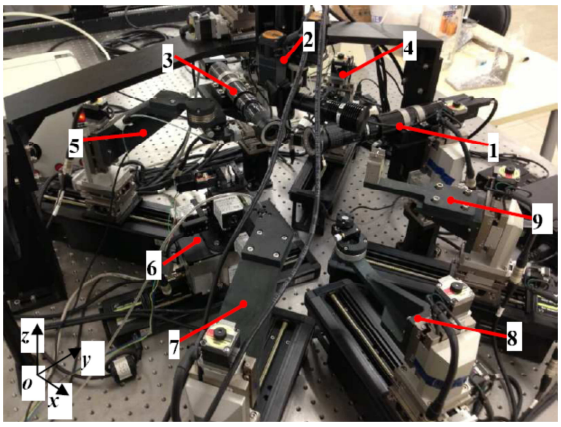

Fig. 6. The assembly platform.

$$\mathbf{A}_4 = \begin{bmatrix} -108.1 & -112.9 & 9.8 & 108.1 & 107.4 & -3.6 \\ -0.6 & 5.2 & 159.6 & -0.5 & -5.6 & -159.2 \end{bmatrix} pixels.$$

The Jacobian matrix of the manipulator 4 in the camera 3 was then calculated as

$${}^3\boldsymbol{J}_4 = \begin{bmatrix} -0.2162 & -0.2203 & 0.0134 \\ -0.0001 & 0.0108 & 0.3188 \end{bmatrix}.$$

Applying the same method to move the manipulator in the view of camera 1 and combining these two matrix yielded the image Jacobian matrix mapping between the manipulator 4 and horizontal microscopes

$${}^h\boldsymbol{J}_4 = \begin{bmatrix} -0.2300 & 0.2235 & -0.0085 \\ -0.0040 & 0.0145 & 0.3180 \\ -0.2162 & -0.2203 & 0.0134 \\ -0.0001 & 0.0108 & 0.3188 \end{bmatrix}.$$

C. The assembly

In the assembly experiments, we set the parameters of hybrid controller as: $\mathrm{K_{p5}} = 0.2$, $\mathrm{K_{i5}} = 0.6$, $f_{Tx} = f_{Ty} = 0.3$N, $f_{Tz} = 2$N, $\lambda_a = 1\mu m$, $\lambda_{bz} = 50\mu m$. The assembly was carried out in a process described in Fig. 2, and Fig. 7 shows the images in different sub-assemblies captured by different microscopes. In Fig. 7(b), the upper object is the end effector of the arm 4 holding the component C. Right now we could achieve the results with errors in alignment within $0.25\mu m$ and 0.05°, and the whole assembly process finished in less than 15 minutes.

Fig. 8 displays the forces between the components A and B during the assembly of interference fit. Horizontal axis is the sampling step of the force sensor. As the insertion went further, the contact area became more, and therefore friction force (along the z-axis) grew larger, gradually reaching 0.85N at the end. Planar forces also grew as the insertion progressed, since the insertion had a long distance (about 1cm) and any deviation from the alignment caused forces during the insertion, as can be seen the black curve in Fig. 8. When the y-axis force reached the threshold, the adjusting mechanism was activated, so that the f_y was around 0.3N and f_x was then lower until the insertion finished.

(a) Assembly of A and B in the view of horizontal cameras

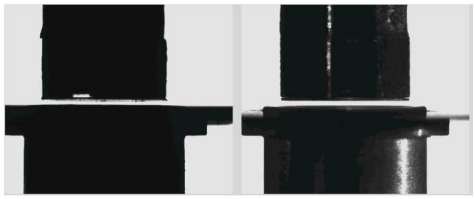

(b) Assembly of A and C in the view of horizontal cameras

(c) Assembly of A and D in the view of cameras 1 and 2

Fig. 7. Each sub-assembly in the view of microscopic vision system.

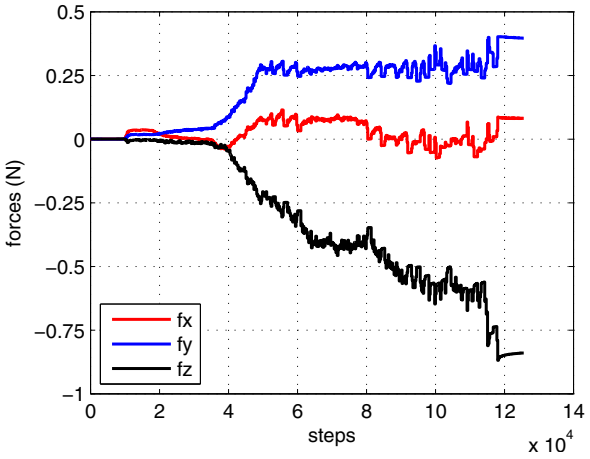

Fig. 8. The forces during insertion between components A and B.

VI. CONCLUSIONS AND FUTURE WORKS

In this paper, a micro-operational platform with multiple manipulators is designed to accomplish a sequence of micro-assembly for irregular components. This study also desires to solve the soft assembly with contact. To reach a high precision and protect the objects, we propose a hybrid control strategy, which incorporates the vision based positioning controller for alignment, the force based insertion controller, and a decision mechanism to switch between controllers. We carried out experiments to show the effectiveness of the proposed platform and control methods.

Future research will implement more experiments to analyze the details in contact micro-assembly between soft objects. We will discuss the proposed control method in a general form to facilitate implementing it in more situations.

ACKNOWLEDGMENT

This work is supported by the Program for National Nature Science Foundation of China (61305115, 61227804).

REFERENCES

[1] M. B. Cohn, K. F. Bohringer, J. M. Noworolski, *et al.*, "Microassembly technologies for MEMS", *Proc. SPIE: Conf. Micro. Dev. Comp*, 1998, pp. 2-16.

[2] M. Savia and H. N. Koivo, "Contact micromanipulation survey of strategies", *IEEE/ASME Trans. Mechatron.*, vol. 14, no. 4, pp. 504-514, 2009.

[3] I. S. Khalil, F. V. Brink, O. S. Sukas, *et al.*, "Microassembly using a cluster of paramagnetic microparticles", *IEEE Int. Conf. Robot. Autom.*, pp. 5527-5532, 2013.

[4] A. Bolopion, H. Xie, D. S. Haliyo, *et al.*, "Haptic teleoperation for 3-D microassembly of spherical objects", *IEEE/ASME Trans. Mechatron.*, vol. 17, no. 1, pp. 116-127, 2012.

[5] N. Dechev, L. Ren, W. Liu, *et al.*, "Development of a 6 degree of freedom robotic micromanipulator for use in 3D MEMS microassembly", *IEEE Int. Conf. Robot. Autom.*, pp. 281-288, 2006.

[6] D. J. Cappelleri and Z. Fu, "Towards flexible, automated microassembly with caging micromanipulation", *IEEE Int. Conf. Robot. Autom.*, pp. 1427-1432, 2013.

[7] J. D. Wason, J. T. Wen, J. J. Gorman, *et al.*, "Automated multiprobe microassembly using vision feedback", *IEEE Trans. Robot.*, vol. 28, no. 5, pp. 1090-1103, 2012.

[8] B. Tamadazte, N. L. Piat, and S. Dembele, "Robotic micromanipulation and microassembly using monoview and multiscale visual servoing", *IEEE/ASME Trans. Mechatron.*, vol. 17, no. 1, pp. 116-127, 2012.

[9] L. Ren, L. Wang, J. K. Mills, *et al.*, "Vision-based 2-D automatic micrograsping using coarse-to-fine grasping strategy", *IEEE Trans. Ind. Electron.*, vol. 55, no. 9, pp. 3324-3331, 2008.

[10] S. J. Koppal, I. Gkioulekas, T. Young, *et al.*, "Towards wide-angle micro vision sensors", *IEEE Trans. Pattern Anal. Mach. Intell.*, vol. 35, no. 12, pp. 2982-2996, 2013.

[11] Y. Wang, D. Li, and C. Liu, "A sereoscopic imaging model and its calibration of micro stereovision for 3D measurement", *Int. Conf. Inform. Acquis.*, pp. 442-447, 2005.

[12] C. C. Cheah, C. Liu, and J. E. Slotine, "Adaptive Jacobian vision based control for robots with uncertain depth information", *Automatica*, vol. 46, no. 7, pp. 1228-1233, 2010.

[13] D. Xing, D. Xu, H. Li, *et al.*, "Active calibration and its applications on micro-operating platform with multiple manipulators", *IEEE Int. Conf. Robot. Autom.*, pp. 5455-5460, 2014.

[14] Q. Xu, "Precision position/force interaction control of a piezoelectric multimorph microgripper for microassembly", *IEEE Trans. Autom. SCI. ENG.*, vol. 10, no. 3, pp. 503-514, 2013.

[15] K. Rabenorosoa, C. Clevy, Q. Chen, *et al.*, "Study of forces during microassembly tasks using two-sensing-fingers grippers", *IEEE/ASME Trans. Mechatron.*, vol. 17, no. 5, pp. 811-821, 2012.

[16] V. Sariola, M. Jaaskelainen, Q. Zhou, *et al.*, "Hybrid microassembly combinging robotics and water droplet self-alignment", *IEEE Trans. Robot.*, vol. 26, no. 6, pp. 965-977, 2010.